EFFECT OF A HEATED DRILLING BIT AND BOREHOLE LIQUID ON THERMOELASTIC STRESSES IN AN ICE CORE

O. V. NAGORNOV[1], V. S. ZAGORODNOV[2] and J. J. KELLEY[2]

[1]*Moscow Engineering Physics Institute, 31 Kashirskoe Shosse, Moscow 115409, Russia*
[2]*Polar Ice Coring Office, University of Alaska Fairbanks, Fairbanks, Alaska 99775-1710, U. S. A.*

Abstract: Thermal ice coring processes are accompanied by stresses in an ice core; micro-and macro-cracks are formed. Contamination under mechanical and thermal drilling usually penetrates from 5 to 30 mm into the ice core. The quality of ice core acquired by thermal drilling depends on thermal stresses. To improve ice core quality, experimental and theoretical studies have been done. A prototype model of an antifreeze thermal electric drill (ATED) was tested. Temperature distribution in an ice core during thermal drilling was measured with thermocouples. To study temperature and stress distributions in an ice core, a mathematical model was developed. Impacts of ethanol-water solution (EWS) and kerosene on temperature and thermal stresses in an ice core were also studied. The experiments and model simulations have shown that thermal stresses in an ice core are proportional to the ratio of drilling bit length to penetration rate. The maximal thermal stresses in an ice core during thermal drilling exhibit only weak dependence on the type of borehole liquid. Forced circulation of the borehole liquid at the kerf leads to reduced depth of cracks by about 10 mm.

1. Introduction

To prevent closure of the borehole, hydrophobic (kerosene, butyl acetate) and hydrophilic (ethanol, ethylene glycol) liquids have been used (UEDA and GARFIELD, 1968; KUDRAYSHOV *et al.*, 1984; GUNDESTRUP, 1989; MOREV and YAKOVLEV, 1984; ZAGORODNOV *et al.*, 1992). Experiments have demonstrated that ethanol and butyl acetate penetrate ice cores to a depth of 30 mm and 3 mm, respectively (GOSINK *et al.*, 1992). Cracks and contamination complicate study of the chemical composition and physical properties of an ice core.

Thermal ice coring is accompanied by heating the subsurface layer of an ice core. Thermoelastic stresses appear in the core, a result of thermal expansion. If thermoelastic stresses are greater than the strength of the ice, micro- and macro-cracks occur. The strength of glacier ice depends on structure, temperature, strain rate, grain size, and other parameters (ANDREWS, 1985; COLE, 1987; GOLD, 1977; HOBBS, 1974; SABOL and SCHULSON, 1989; SCHULSON *et al.*, 1989a,b; TIMCO and FREDERKING, 1982). At strain rate higher than approximately $2 \cdot 10^{-2}$ s^{-1} the most probable tensile and compressive strengths of ice are about 1–2 MPa and 2–4 MPa, respectively. The strength of artificial ice subjected to thermal shock was found to be between 3 and 4 MPa (GOLD, 1963). Cracks in glacier ice core recovered by thermal drilling occur at temperatures below −10°C.

The segment of ice core shown in Fig. 1a was obtained from the Academy of Sciences glacier (Severnaya Zemlya) at a depth of 300 m and at ice temperature $T_i = -14$°C using an antifreeze thermal electrical drill (ATED) (ZAGORODNOV, 1989). The ice core was broken into 2- to 10-cm pieces. The other piece of ice core (Fig. 1b) was obtained at Mizuho station from a depth of 356 m, where $T_i = -45$°C, by a thermal drill in a dry borehole

a   b
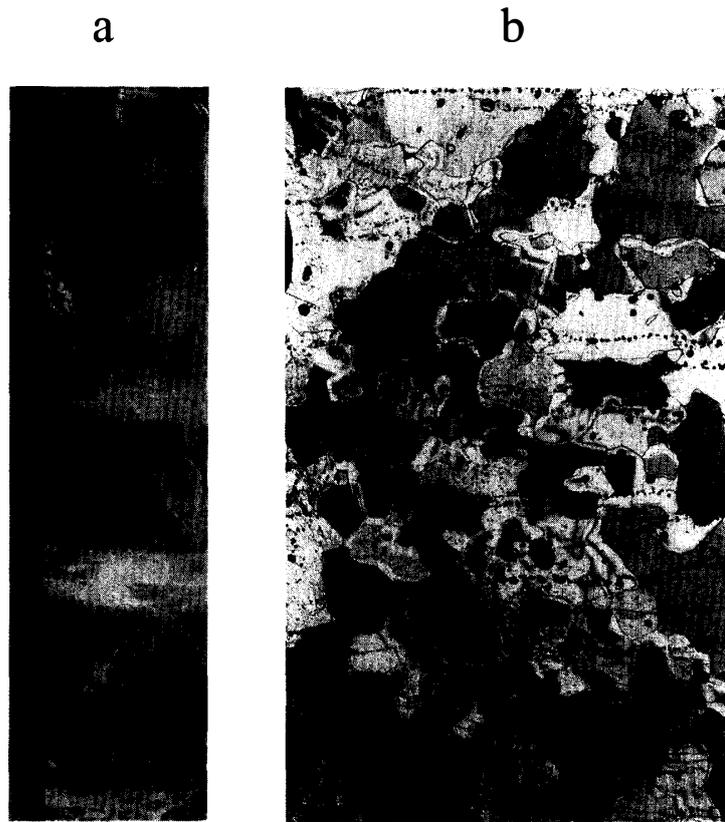
Fig. 1.   Segment of the ice core taken with ATED (a) at T=-14°C and (b) a vertical thin section (3.5 × 2.5 cm) of an ice core obtained by a conventional thermal drill at T_i=-45°C.

(NARITA et al., 1985; FUJII, 1978).   The distance between the cracks was 0.5 to 3 mm. Sub-horizontal, slightly convex, downward cracks are most often observed in ice cores. Inclined cracks are rarely found. Uniaxial compression experiments at -10°C at 10^{-3} s^{-1} on
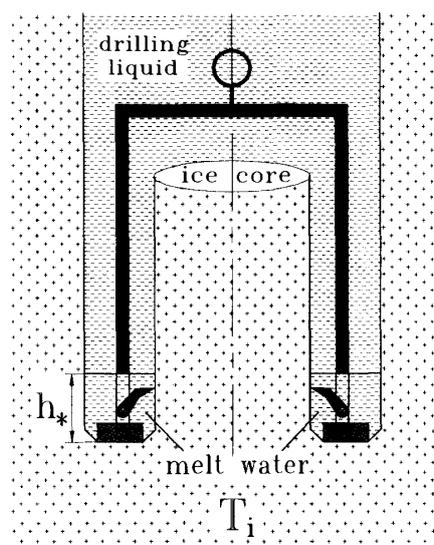
Fig. 2.   Schematic of a thermal drill.

fresh-water ice cores have shown uniform distribution of cracks and axial splitting (SCHULSON et al., 1989). The uniaxial tension testing of cored ice specimens demonstrates sub-horizontal fracture (LEE, 1986; SABOL and SCHULSON, 1989). The preferential sub-horizontal cracking suggests extension loading of the ice core during thermal drilling.

A schematic of a conventional thermal ice core drill is shown in Fig. 2. The inner space of the core barrel is connected to the borehole through the core catcher's windows. Therefore, the meltwater level on the kerf inside and outside of the drilling bit remains the same. Depending on the thermal drill structure and drilling regimes, the water level varies from 5 to 75 mm (AUGUSTIN et al., 1989; BIRD, 1976; SUZUKI, 1976). During ATED drilling the meltwater is mixed with hydrophilic antifreeze at the kerf and retained in the borehole. The water level is about 50 mm. The goal of the present study is to investigate the effect of heat transfer during thermal electrical drilling, resulting in ice core fracture.

2. Experimental Investigations of the Temperature Regime of Ice and EWS under Thermal Drilling

The scheme and specification of the experimental stage for measuring temperatures during thermal drilling are presented in Fig. 3 and Table 1. A driving bar was used to keep the drill at a fixed distance from thermocouples deployed in the ice. An ATED was used in the experiments (BOGORODSKY and MOREV, 1984; ZOTIKOV, 1979). The ATED model has a layer of insulation to decrease heating of the core by the drilling fluid. The thermo-
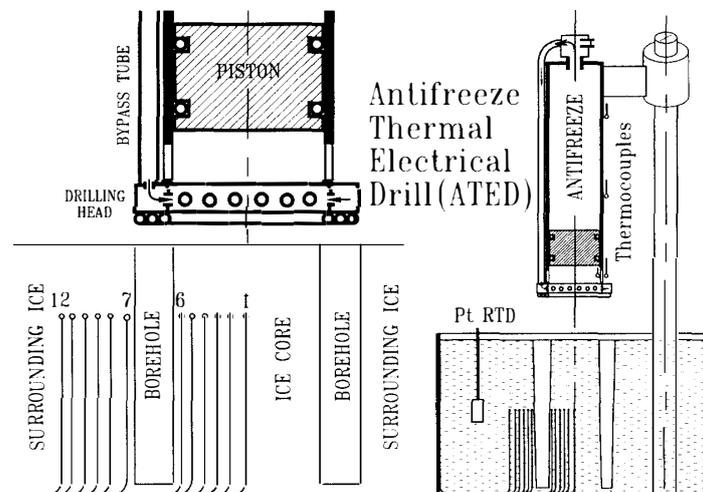
Fig. 3. Schematic of experimental stage.

Table 1. Specification of experimental stage.

Depth of drilling	258 mm
Diameter of drilling bit (inner/outer)	89/102 mm
Average diameter of the ice core/borehole	84/104 mm
Power of drilling bit	700 W
Speed of drilling	0. 7 mm s^1

electric drill bit (5 mm high) developed by PICO (KOCI, 1985, 1989) was applied. As the ice core pushes the piston, antifreeze (EWS) is pumped up to the kerf.

The temperature of the ice was measured by eleven thermocouples (TP) and Platinum Resistance Temperature Detectors (PRTD) placed into the ice block. One TP was mounted inside and three TP were outside of the core barrel (Fig. 3). These allowed measurement of the EWS temperature during drilling. A commutator scanned the thermocouples with a frequency of 0.25 Hz. Output voltage from the thermocouples was registrated by a strip chart recorder. Resistance of the PRTD was measured by a digital multimeter. The accuracy of the TP measurements was +0.25°C and the accuracy of the PRTD was +0.1°C.

If the power is constant, then the drilling speed is stable. The vertical position of the drill relative to the thermocouples was defined as a product of time and drilling speed. When the drill had penetrated into the ice block, the drilling bit was turned off. The drill was left in the borehole for 40 min. Thus, conditions of thermal impact on an ice core during one run were reproduced. The experimental stage was placed into a freezer and held at a constant temperature of –13.5°C. Three drilling experiments were carried out: (1) drilling with meltwater at the kerf; (2) with 95% EWS and water level (h.) of 30 mm; and (3) EWS and h.=5 mm.

The results of temperature measurements are shown in Figs. 4 and 5. Some disagreement between estimated and observed values are explained both by errors of temperature measurement and assumptions of the mathematical model. Temperature distribution of EWS during drilling is shown in Fig. 5. Based on data in Fig. 5 one may assume that at ≃0.4 m above the kerf the EWS temperature approaches T_i. The measured temperature difference of EWS inside and outside the core barrel was about 2°C. To simulate ice-EWS interaction, latent heat of ice dissolution was measured by a calorimeter (NAGORNOV et al., 1993).
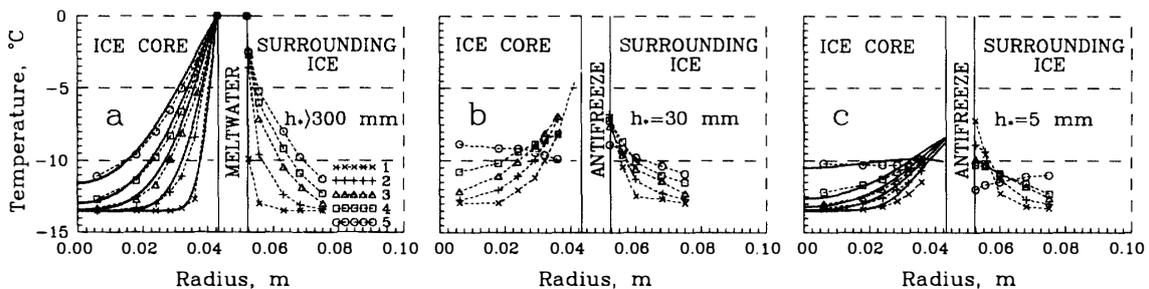
Fig. 4. Experimental and calculated (solid lines) temperature distribution in ice during thermal drilling with water (1–5: t=10, 40, 80, 120 and 440 s).
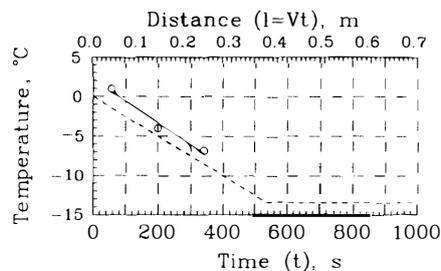
Fig. 5. Temperature of EWS: solid line is outer surface of the core barrel, dashed line is inner surface; l=0 is the bottom of the drilling bit.

3. Mathematical Model of Temperature Regime of an Ice Core during Thermal Drilling

Assume an ice core to be a cylinder. The drilling bit transfers heat to an ice core radially through the film of meltwater (Fig. 2). During contact with the meltwater the ice core is heated. The time of ice core heating is $t_* = h_*/V_d$, where V_d is drilling speed and h_* is the meltwater level at the kerf. About 1 mm to 2 mm of ice core melts radially. It is significantly less than the radius of the ice core. Therefore, it can be ignored while modeling heat and mass transfer in an ice core. Temperature changes along the radius are essentially greater than along an ice core axis. Thus, a one-dimensional approximation of heat transfer is adopted to describe the temperature regime of an ice core. Temperature of an ice core $T(r, t)$ is governed by the equation of energy balance:

$$\frac{\partial T}{\partial t} = \chi_i \left(\frac{\partial^2 T}{\partial r^2} + \frac{1}{r} \frac{\partial T}{\partial r} \right), \qquad t > 0, 0 < r < R \tag{1}$$

where χ_i is the thermal diffusivity of ice, r is the radial coordinate, and R is a radius of an ice core. Thermal flux is equal to zero along the ice core axis:

$$\frac{\partial T}{\partial r} = 0. \qquad t > 0, r = 0 \tag{2}$$

At the lateral boundary of the ice core, the temperature is defined by

$$T(R, t) = T_w, \qquad t > 0 \tag{3}$$

where T_w is the ice melting temperature. The initial temperature in an ice core is given by

$$T(r, 0) = T_i. \qquad 0 < r < R \tag{4}$$

Equations (1) through (4) were solved using finite-difference expansions of derivatives and an unconditionally stable implicit scheme, second-order accurate in time and coordinate. This solution is found at $0 < t < t_*$. A similar solution is obtained for the surrounding ice. The following parameters were specified in model simulations: $R = 0.043$ and 0.05 m, $T_i = -13.5°$, $-25°$, $-30°$, and $-60°C$, $\chi_i = (1.0...1.2) \cdot 10^{-6}$ m^2 s^{-1}. Temperature distribution in the ice core is presented in Fig. 4a.

3.1. Hydrophobic drilling liquid

At $t = t_*$ the lateral surface of the ice core contacts the drilling liquid. Due to heating by the drilling bit, the temperature of the drilling liquid is higher than the temperature of the ice core. If the temperature of the hydrophobic drilling fluid is lower than the ice melting point, the heat flux in the radial direction can be represented by a continuous function. Boundary conditions at the lateral surface of the ice core and at the borehole wall are:

$$k_i \frac{\partial T}{\partial r} = k_k \frac{\partial T}{\partial r}, \qquad t > t_*, r = R \tag{5}$$

$$k_k \frac{\partial T}{\partial r} = k_i \frac{\partial T}{\partial r}, \qquad t > t_*, r = R_b \tag{6}$$

where k_i and k_k are thermal conductivity of ice and hydrophobic liquid, respectively, and R_b is the borehole radius. The temperature of the hydrophobic liquid at $R < r < R_b$ is described by the equation:

$$\frac{\partial T}{\partial t} = \chi_k \left(\frac{\partial^2 T}{\partial r^2} + \frac{1}{r} \frac{\partial T}{\partial r} \right), \qquad t > t_*, R < r < R_b \tag{7}$$

where χ_k is the thermal diffusivity of the hydrophobic liquid. At $r > R_b$ the temperature of the ice can be determined by eq. (1). The temperature distribution at $t = t_*$ is used as the initial condition. Equations (5) through (7) were solved similar to eq. (1) through (4). These problems are similar: if the initial temperature of the ice $T(r, 0)$ is increased or decreased, then $T(r, t)$ would increase or decrease as much.

For example, here are the thermal effects of kerosene. For modeling, the following parameters were used: k_i=2.3...2.7 J/(m·s·°C), k_k=0.116 J/(m·s·°C), R=0.05 m, R_b=0.062 m, χ_k=0.62·10^{-7} m^2 s^{-1}; t_*=5 and 30 s; T_k=0°C; T_i=−60°C. The calculated temperature distributions are shown in Fig. 6a.

3.2. Hydrophilic drilling liquid

Let us consider EWS as a drilling liquid. The temperature of the ice core surface at $t = t_*$ is the melting point. If the concentration of EWS is higher than C_{eq}, then an ice core dissolution occurs. Concentration $C(r, t)$ and temperature of EWS $T(r, t)$ are governed by the following equations:

$$\frac{\partial C}{\partial t} = D \left(\frac{\partial^2 C}{\partial r^2} + \frac{1}{r} \frac{\partial C}{\partial r} \right), \qquad t > t_*, R < r < R_d \tag{8}$$

and

$$\frac{\partial T}{\partial t} = \chi_s \left(\frac{\partial^2 T}{\partial r^2} + \frac{1}{r} \frac{\partial T}{\partial r} \right), \qquad t > t_*, R < r < R_d \tag{9}$$

where χ_s is thermal diffusivity of the solution and D is the diffusion coefficient. On the lateral surface of an ice core ($r = R$), thermal flux is defined by the equation:

$$k_s \frac{\partial T}{\partial r} - k_i \frac{\partial T}{\partial r} = \lambda \rho \frac{dR}{dt}, \qquad t > t_*, r = R \tag{10}$$

where k_s is thermal conductivity of the EWS, λ is the latent heat of ice dissolution, and ρ is ice density. The EWS concentration at the ice core surface yields:

$$C(R, t) = C_{eq}(T). \tag{11}$$

The mass flux of ethanol at the ice core surface is determined by the mass balance equation:

$$-D \frac{\partial C}{\partial r} = C \frac{dR}{dt}. \qquad t > t_*, r = R \tag{12}$$

Taking into account the 2°C temperature difference inside and outside of the core barrel (Fig. 6), the temperature distribution of the EWS at the inner surface of the core barrel (T_d) becomes
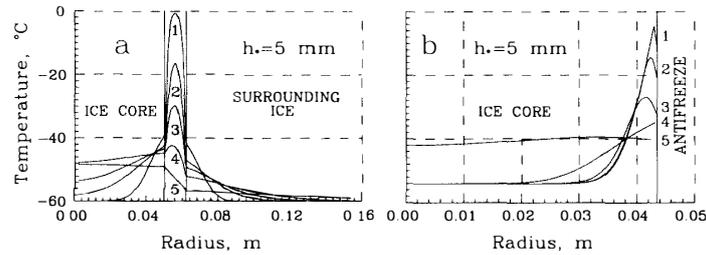
Fig. 6. Calculated temperature distribution in ice during thermal coring: (a) with kerosene (1-5: t=34, 173, 325, 653 and 3600 s) and (b) with EWS (1-5: t=0.05, 0.6, 3.5, 25 and 433 s).

$$T(R_d, t) = T_d(t), \qquad t > t_* \qquad (13)$$

$$\text{where } T_d(t) = \begin{cases} -0.025{\cdot}t, & 0 < t < 540 \\ -13.5. & t > 540 \end{cases}$$

There is good agreement between calculated and measured temperatures in subsurface layers of the ice core (Fig. 4).

On the inner surface of the core barrel, the mass flux of ethanol is:

$$\rho D \frac{\partial C}{\partial r} = 0, \qquad t > t_*, r = R_d \qquad (14)$$

The distribution of temperature at $t = t_*$ is used as an initial condition. The initial concentration of EWS is specified as:

$$C(r, 0) = C_o = 0.95. \qquad R < r < R_d \qquad (15)$$

Equations (1), (2), and (8) through (15) were solved using finite-difference expansions of derivatives; care was taken to retain equal accuracy in the first-order and second-order spatial derivatives in the equations. A Crank-Nichelson implicit scheme, second-order accurate in time, was applied. The phase boundary position is determined by the iteration method. For modeling, the following parameters where used: R=0.043 and 0.05 m, R_d=0.04375 m, T_i= $-13.5°$, $-30°$ and $-60°$C, χ_i=(1.0...1.2) $\cdot 10^{-6}$ m^2 s^{-1}, χ_s=(0.4...1.1) $\cdot 10^{-7}$ m^2 s^{-1}, D=(0.1...1.0) $\cdot 10^{-8}$ m^2 s^{-1}, λ =30, 100, 220 kJ kg^{-1}, ρ =920 kg m^{-3}, k_i=2.3...2.7 J/(m·s·°C), k_s=0.2...0.27 J/(m·s·°C).

The distribution of temperature in an ice core during ice-EWS interaction is given in Figs. 4b, c and 6b. Intensive cooling of the subsurface layer of the ice core lasted about ten seconds (Fig. 6b). Subsurface cooling results from of heat dissipation from EWS and ice dissolution. Moreover, heat extraction by conductivity from the ice core also takes place. The experiment did not reveal non-monotonous temperature dependence since the closest thermocouple was 6.5 mm away from the lateral surface of the ice core. As hydrophobic liquids do not dissolve ice, heat dissipation occurs only through conductivity. Modeling and experiments can determine the temperature dependence of the center of an ice core during thermal drilling (Fig. 7). During the first 400 s, heating of the ice core only weakly depends on the type of drilling liquid. At t =2000 s the temperature of the ice core center approaches initial ice temperature. The temperature drops relatively rapidly during ATED drilling due to dissolution and heat conduction; slower cooling of the ice core by kerosene results from its low thermal conductivity.
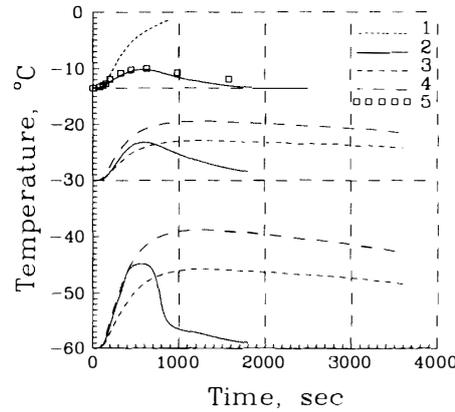
Fig. 7.   Temperature at center of the ice core affected by borehole fluids: 1–water, 2–EWS,
3–kerosene (h.=5 mm), 4–kerosene (h.=30 mm), 5–experimental data.

4. Thermoelastic Stresses in Ice Core

Thermoelastic stresses in an ice core arise from heating. The speed of thermal drilling V_d is lower than the speed of elastic waves in the ice. Thus, modeling of thermoelastic stresses can be done without consideration of wave phenomenon. The momentum balance is governed by the equation:

$$\frac{3\,(1-v)}{1+v}\,\frac{d}{dr}\,(\frac{1}{r}\,\frac{d}{dr}\,(ru)) = \alpha\,\frac{dT}{dr}\,, \tag{16}$$

here v is the Poisson coefficient of ice, α is the coefficient of volume expansion of ice and u is radial displacement of ice (LANDAU and LIFSHITS, 1965). Here the temperature T is higher than T_i. Obviously, the radial stress at the ice core surface is $\sigma_r\,(R)=0$. Using calculated temperature distribution $T\,(r)$, eqs. (16) and (18) for radial displacement can be derived:

$$u\,(r) = \alpha\,(1+v)\,/\,(3\,(1-v))\,(1/r \int_0^r T\,(s)\,sds + (1-2v)\,r/R^2 \int_0^R T\,(s)\,sds), \tag{17}$$

where s is the integration variable. Then the radial stress (σ_r) becomes:

$$\sigma_r = E\alpha\,/\,(3\,(1-v))\,(1/R^2 \int_0^R T\,(s)\,sds - 1/r^2 \int_0^r T\,(s)\,sds), \tag{18}$$

where elastic modulus $E=(1-v^2)\,\rho c^2$, c is the speed of longitudinal elastic waves. The angular and axial components of the stress tensors σ_ϕ and σ_z are given by:

$$\sigma_\phi = E\alpha/\,(3\,(1-v))\,(1/r^2 \int_0^r T\,(s)\,sds + 1/R^2 \int_0^R T\,(s)\,sds - T\,(r)), \tag{19}$$

$$\sigma_z = E\alpha/\,(3\,(1-v))\,(2v/R^2 \int_0^R T\,(s)\,sds - T\,(r)). \tag{20}$$

The model was applied to calculate thermoelastic stresses in the ice core taken with conventional thermal drills which were operated with kerosene and ATED. Two types of ATED drills were modeled: (1) with a short drilling bit (h_*=5 mm); and (2) the same bit with forced circulation of the EWS (h_*=0.5 mm).

The greatest thermoelastic stresses are expected at low temperature (T_i= -60°C). Consider the axial stress (σ_z) in an ice core during thermal drilling (Fig. 8). At the beginning of coring the σ_z and σ_Φ components have their greatest values (0-40 MPa) in the 4- to 6-mm thick subsurface layer of an ice core. In this layer σ_z and σ_Φ exceed the compressive strength of ice. The radial component of the stress σ_r=0 at the ice core surface. In the central portion of the ice core the σ_r, σ_z and σ_Φ are tensile stresses. When ice core heating continues, the direction and values of the stresses are changed. The maximum values of compression thermal stress occur after 500-1000 s of drilling.
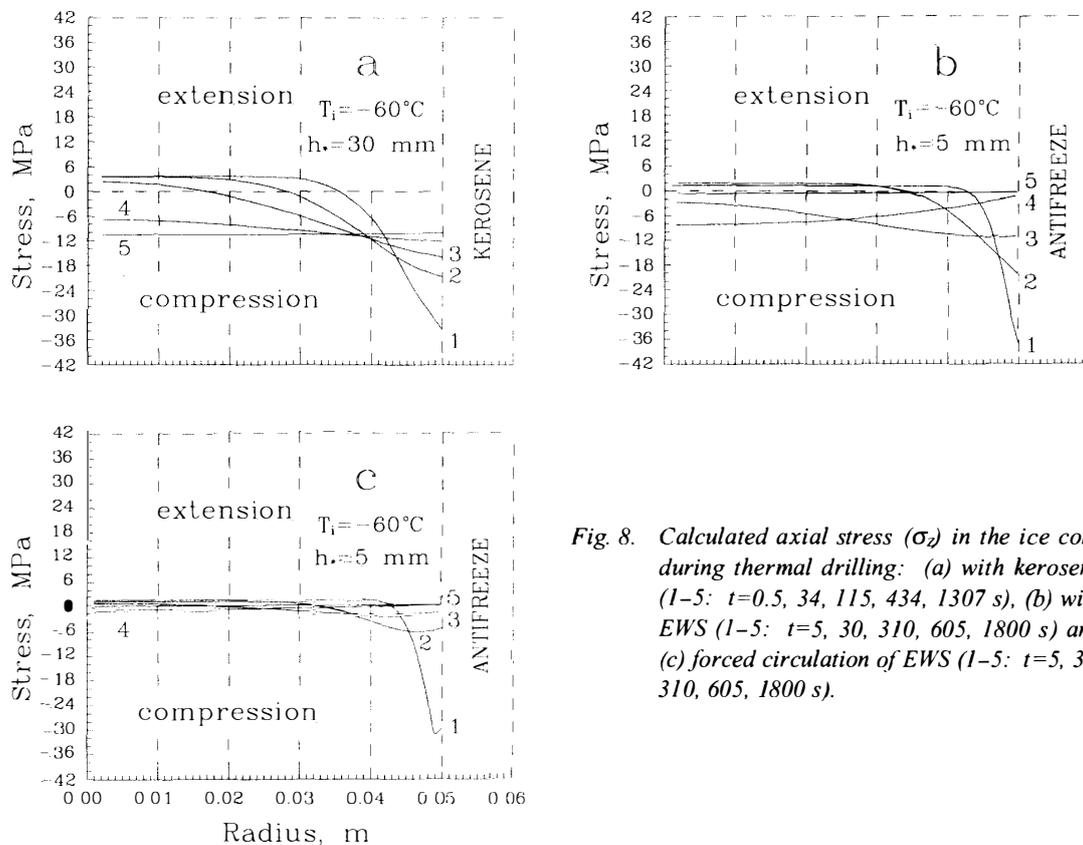
Fig. 8.   Calculated axial stress (σ_z) in the ice core during thermal drilling: (a) with kerosene (1-5: t=0.5, 34, 115, 434, 1307 s), (b) with EWS (1-5: t=5, 30, 310, 605, 1800 s) and (c) forced circulation of EWS (1-5: t=5, 30, 310, 605, 1800 s).

During ice-EWS interaction the ice core cools and stresses decrease. The center of an ice core becomes almost isothermal at t_{iso}=440 s (Fig. 4b). At this moment the axial stresses level off along the radius of the ice core and become equal to about 2 MPa. The same model has been used for simulation of an ice core-EWS and ice core-kerosene interaction. The values of the σ_z along the ice core (Fig. 8a) slightly exceed the corresponding values in the former case (Fig. 8b). Hence, the model simulations show that in both cases thermal stress significantly exceeds the strength of the ice in the subsurface layer of the ice core. On the contrary, stresses in the center of the ice core are close to or slightly exceed the strength of ice. Contamination penetrates to a depth of up to 30 mm

from the surface of the ice core (BOUTRON *et al.*, 1989; GOSINK *et al.*, 1991, 1992). The maximum concentration of contamination is found at about the 5–10 mm subsurface layer of the ice core. Thus, depth of contamination and maximum stress appear to be closely related.

The model also demonstrated that the value of the thermal stress depends on the height of the meltwater at the kerf. The less the h_*, the less thermal stress (Figs. 4 and 8). Increased drilling speed also decreased thermal stress.

It is apparent then that the drilling fluid determines the temperature regime and the magnitude of thermoelastic stresses in the ice core. To decrease the thermoelastic stresses it is necessary to decrease the drilling fluid temperature. Such a drilling regime can be accomplished by forced circulation of the drilling fluid at the kerf. To provide this regime, drilling fluid at temperature T_i can be pumped from the top of the drill to the kerf. Therefore, the temperature of the ice core surface will be close to T_i. Heat from the kerf zone will be removed by the drilling liquid and absorbed by the borehole wall.

Thermal coring with forced circulation of EWS at $T = -60°C$ has been modeled. It was found that maximum tensile and compressive stresses in the center of an ice core are about 0.5 and 1.5 MPa, respectively (Fig. 8c). The depth of the thermal stress exceeding 2 MPa is about 10 mm. Thus, the cracks may form only at the subsurface layer. It is expected that ethanol contamination of the ice core recovered under the described drilling regime would be significantly reduced.

5. Conclusions

1) Under thermal ice coring at temperatures below $-10°C$ subhorizontal cracks are formed. The main cause of ice core fracture is thermal stresses occurring due to the effect of the heated drilling bit and drilling liquid. The shorter the length of the drilling bit and the depth of the meltwater at the kerf, the less the ice core is heated.

2) Use of kerosene as the drilling fluid under conventional drilling procedures provides approximately the same magnitude of thermal stresses in an ice core as EWS with ATED.

3) At temperature $-60°C$, forced circulation of EWS at the kerf can reduce the thermal stresses in an ice core by a factor of 5–6. The expected depth where stress exceeds tensile strength of ice (2 MPa) is about 10 mm. Thus, modification of the ATED enables retrieval of the ice core at $T_i = -60°C$ with a contaminated layer of 10 mm.

Acknowledgments

References

ANDREWS, R.M. (1985): Measurement of the fracture toughness of glacier ice. J. Glaciol., **31**, 171–176.

Augustin, L., Donnou, D., Rado, C., Manouvrier, A., Girard, C. and Ricou, G. (1989): Thermal ice core drilling. Ice Core Drilling; Proceedings of the Third International Workshop on Ice Drilling Technology, Grenoble, France, Oct. 10–14, 1988, ed. by C. Rado and D. Beaudoing. Grenoble, Centre National de la Recherche Scientifique, Laboratoire de Glaciologie et Geophysique de l'Environment, 59–65.

Bird, I.G. (1976): Thermal ice drilling: Australian developments and experience. Ice-Core Drilling; Proceedings of a Symposium, University of Nebraska, Lincoln, 28–30 August 1974, ed. by J.F. Splettstoesser. Lincoln, University of Nebraska Press, 1–18.

Bogorodsky, V.V. and Morev, V.A. (1984): Equipment and technology for drilling in temperate glaciers. CRREL Spec. Rep., 84-34, 129–132.

Boutron, C.F., Patterson, C.C. and Barkov, N.I. (1989): Assessing the quality thermal drilling antarctic ice cores for trace elements analysis. Ice Core Drilling; Proceedings of the Third International Workshop on Ice Drilling Technology, Grenoble, France, Oct. 10–14, 1988, ed. by C. Rado and D. Beaudoing. Grenoble, Centre National de la Recherche Scientifique, Laboratoire de Glaciologie et Geophysique de l'Environment, 182–197.

Cole, D.M. (1987): Strain-rate and grain-size effects in ice. J. Glaciol., 33, 274–280.

Fujii, Y. (1978): Temperature profile in the drilled hole. Mem. Natl Inst. Polar Res., Spec. Issue, 10, 169.

Gold, L.W. (1963): Crack formation in ice plates by thermal shock. Can. J. Phys., 41, 1712–1728.

Gold, L.W. (1977): Engineering properties of fresh-water ice. J. Glaciol., 19, 197–212.

Gosink, T.A., Tumeo, M.A., Koci, B.R. and Burton, T.W. (1991): Butyl acetate, an alternative drilling fluid for deep ice-coring projects. J. Glaciol., 37, 170–176.

Gosink, T.A., Koci, B.R. and Kelley, J.J. (1992): Aqueous ethanol as an ice drilling fluid. J. Glaciol. (in press).

Gundestrup, N.S. (1989): Hole liquids. Ice Core Drilling; Proceedings of the Third International Workshop on Ice Drilling Technology, Grenoble, France, Oct. 10–14, 1988, ed. by C. Rado and D. Beaudoing. Grenoble, Centre National de la Recherche Scientifique, Laboratoire de Glaciologie et Geophysique de l'Environment, 51–53.

Hobbs, P.V. (1974): Ice Physics. Oxford, Clarendon Press, 837 p.

Koci, B. (1985): Instruments and methods: Ice core drilling at 5700 m powered by a solar voltaic array. J. Glaciol., 31, 360–361.

Koci, B. (1989): Design of a drill to work in a fluid filled hole. Ice Core Drilling; Proceedings of the Third International Workshop on Ice Drilling Technology, Grenoble, France, Oct. 10–14, 1988, ed. by C. Rado and D. Beaudoing. Grenoble, Centre National de la Recherche Scientifique, Laboratoire de Glaciologie et Geophysique de l'Environment, 28–31.

Kudrayshov, B.B., Chistyakov, V.K., Pashikevich, V.M. and Petrov, V.N. (1984): Selection of a low temperature filler for deep holes in the Antarctic Ice Sheet. CRREL Spec. Rep., 84-34, 137–138.

Landau, L.D. and Lifshits, E.M. (1965): Elasticity Theory. Moscow. Nauka. (in Russian).

Lee, R. (1986): A procedure for testing cored ice under uniaxial tension. J. Glaciol., 32, 540–541.

Morev, V.A. and Yakovlev, V.M. (1984): Liquid fillers for bore holes in glaciers. CRREL Spec.Rep., 84-34, 133–135.

Morev, V.A., Manevskiy, L.N., Yakovlev, V.M. and Zagorodnov, V.S. (1989): Drilling with ethanol-based antifreeze in Antarctic. Ice Core Drilling; Proceedings of the Third International Workshop on Ice Drilling Technology, Grenoble, France, Oct. 10–14, 1988, ed. by C. Rado and D. Beaudoing. Grenoble, Centre National de la Recherche Scientifique, Laboratoire de Glaciologie et Geophysique de l'Environment, 110–113.

Nagornov, O. V., Zagorodnov, V. S. and Kelley, J. J. (1993): Interaction of hydrophilic liquid with ice. Proceedings of the Fourth International Symposium on Thermal Engineering and Science for Cold Regions, 28 Sept.–1 Oct. 1993, Hanover, New Hampshire, U. S. A., 160–169.

Narita, H., Nakayama, Y.M., Nakawo, M. and Suzuki, Y. (1985): Intermediate-depth and shallow core drilling operations in Mizuho Plateau, Antarctic, in 1983-84 field season (abstract). Mem. Natl Inst. Polar Res., Spec. Issue, 39, 249–250.

Sabol, S.A. and Schulson, E.M. (1989): The fracture toughness of ice in contact with salt water. J. Glaciol., 35, 191–192.

Schulson, E.M., Hoxie, S.G. and Nixon, W.A. (1989a): The tensile strength of cracked ice. Philos. Mag. A, 59, 303–311.

Schulson, E.M., Gies, M.C., Lasonde, G.L. and Nixon, W.A. (1989b): The effect of the specimen-platen interface on internal cracking and brittle fracture of ice under compression: high-speed photography. J. Glaciol., 35, 378–382.

SUZUKI, Y. (1976): Deep core drilling by Japaneese Antarctic Research Expeditions. Ice-Core Drilling; Proceedings of a Symposium, University of Nebraska, Lincoln, 28–30 August 1974, ed. by J.F. SPLETTSTOESSER. Lincoln, University of Nebraska Press, 155–166.

TIMCO, G.W. and FREDERKING, R.M.W. (1982): Comparative strengths of fresh water ice. Cold Reg. Sci. Technol., **6**, 21–27.

UEDA, H.T. and GARFIELD , D.E. (1968): Core drilling through the Antarctic ice sheet. CRREL Tech. Rep., **231**, 18p.

ZAGORODNOV, V.S. (1989): Antifreeze-thermodrilling of cores in Arctic Sheet Glaciers. Ice Core Drilling; Proceedings of the Third International Workshop on Ice Drilling Technology, Grenoble, France, Oct. 10–14, 1988, ed. by C. RADO and D. BEAUDOING. Grenoble, Centre National de la Recherche Scientifique, Laboratoire de Glaciologie et Geophysique de l'Environment, 97–109.

ZAGORODNOV, V.S., MOREV, V.A., NAGORNOV, O.V., KELLEY, J.J., GOSINK, T.A. and KOCI, B.R. (1992): Hydrophilic liquid in glacier boreholes. Polar Ice Coring Office, Tech. Rep. **92-3**, University of Alaska Fairbanks, 33.

ZOTIKOV, I.A. (1979): Antifreeze-thermodrilling for core through the central part of the Ross Ice Shelf (J-9 Camp), Antarctic. CRREL Rep., **79-24**, 12p.

List of Symbols

$C=C(r, t)$	mixture concentration
$C_{eq}(T)$	equilibrium concentration
c	speed of longitudinal elastic waves in ice
D	diffusivity coefficient
E	elastic modulus (Young's modulus)
h_*	height of water level above kerf
k_i	thermal conductivity of ice
k_k	thermal conductivity of kerosene
k_s	thermal conductivity of solution
R	radius of the ice core
R_b	radius of borehole
R_d	radius of core barrel
r	radial coordinate
s	integration variable
T	temperature
T_i	initial temperature of ice core
T_w	temperature of ice melting
t	time
t_*	time of ice core heating
t_{iso}	time when the ice core becomes isothermal
u	radial displacement
V_d	the rate of drilling-melting
α	coefficient of volume expansion of ice
λ	the latent heat of ice dissolution
ν	Poisson coefficient
ρ	density of ice
σ_r	radial stresses
σ_z	axial stresses

σ_Φ	angular stresses
χ_i	thermal diffusivity of ice
χ_k	thermal diffusivity of kerosene
χ_s	thermal diffusivity of ethanol-water solution
T_k	temperature of kerosene at $t = t_*$

Sub-indexes characterize:

i	ice
s	ethanol-water solution
k	kerosene